THE EFFECT OF ROTATION ON THE GROWTH OF HAIRPIN VORTICES IN SHEAR FLOWS. NUMERICAL SIMULATIONS

Moshe Rosenfeld
Faculty of Engineering, Tel Aviv University, Tel Aviv 69978, Israel

Jacob Cohen and Vladimir Levinski
Faculty of Aerospace Engineering, Technion, Haifa 32000, Israel

ABSTRACT

Hairpin vortices are basic flow structures of turbulent boundary layers and therefore their study is of great importance. One of the basic steps for understanding the mechanisms that govern turbulent boundary layers is to consider the evolution of a *single* hairpin vortex. This may contribute eventually not only to the comprehension of the hairpin creation processes and to a better understanding of turbulent boundary layers, but also to devising means for controlling boundary layer turbulence by taming hairpins. In the present study, a numerical model of an experimental setup was built. An initial disturbance was created by suction. Numerical simulations of the inception, growth and shedding of hairpin vortices in laminar rotating shear flows were compared with experimental results to validate the numerical model. In the instability region, the disturbance grows in size until it becomes a hairpin that is eventually shed, while another hairpin is being formed. The numerical results are in good agreement with the experimental results. The validated numerical model is suitable for future study of the mechanisms involved in the hairpin vortex evolution and shedding.

INTRODUCTION

In the present paper the evolution of finite-amplitude localized disturbances in laminar rotating shear flows is numerically investigated. This is a sequel to the theoretical and experimental contributions of Levinski & Cohen (1995) and Malkiel, Levinski & Cohen (1999), respectively.

In 1967, Kline *et al.* revealed hairpin like well organized vortex structures in the near wall region of a turbulent boundary layer. Following this pioneering work, these structures were reported by a growing list of researches that suggested hairpin type vortices as one of the basic flow structures of turbulent boundary layers. Hairpin vortices consist of a pair of counter-rotating 'legs' inclined to the main flow direction and connected by a relatively short 'head' segment. Numerous experimental and computational works identified hairpin vortices in shear flows, see for example Head and Bandyopadhyay (1981) and Moin and Kim (1985). All these cases considered a large population of hairpin vortices. Zhou *et al.* (1996) showed that sufficiently strong hairpin vortices generate a hierarchy of secondary hairpin vortices, providing the mechanism by which the vortices reproduce themselves and eventually populate the entire near wall region.

Thus, one of the basic steps for understanding the mechanisms that govern turbulent boundary layers is to consider the evolution of a *single* hairpin vortex. This may contribute eventually not only to the comprehension of the hairpin creation processes and to a better understanding of turbulent boundary layers, but also to devising means for controlling boundary layer turbulence by taming hairpin vortices.

To understand the mechanism leading to the rapid growth of a hairpin vortex in boundary layers, Levinski & Cohen (1995) focused on the evolution of a localized disturbance, all dimensions of which are much smaller than the length scale characterizing variations of the basic (unperturbed) flow. According to the results of the theoretical model, planar unidirectional flows are always unstable with respect to finite-amplitude localized disturbances. For this reason, in their experimental work Malkiel *et al.* (1999) focused on an axisymmetric Couette flow for which a stability criterion is predicted to exist. Moreover, unlike plane shear flows in which the inclination angle of the growing vortex is predicted to be 45°, this angle in the case of rotating shear flows is found theoretically to be a function of the basic flow parameters.

It was found that the theoretical predictions concerning the marginal value for instability are in good agreement with the experimental observations. In addition, measurements of the inclination angles of hairpin vortices under various external

flow conditions showed good qualitative agreement with the theoretical predictions. Based on the experimental results, it was concluded that the theoretical criterion is sufficient in predicting stability, i.e. it is capable of determining the conditions under which the initial vortex disturbance will not grow. However, the experimental results show that the model provides only a necessary condition for instability. Thus, for instability to occur, more conditions associated with the initiation of the vortical disturbance need to be satisfied.

CFD simulations can be utilized to study the physics of the hairpin evolution. It can provide high resolution description of both the velocity and pressure fields. Moreover, CFD techniques can be used to isolate parameters easily, and thus shed light on the underlying flow processes. The experiments considered the evolution of a single hairpin in a laminar flow. Therefore, the computational task is of reasonable extent; a single hairpin can be resolved with a higher resolution than in many existing DNS or LES studies that considered a large number of hairpin vortices.

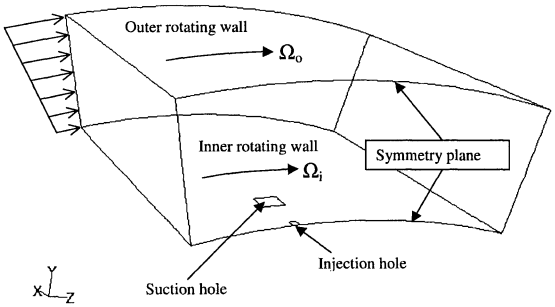

Figure 1: The computational domain

Yet, the accuracy and validity of the numerical simulations should be demonstrated first. The present study focuses on the verification of the numerical model and the numerical solution. The specific objectives of the present numerical study are (i) to validate the numerical simulations with the experimental results; this will allow the future use of numerical simulations in investigating conditions for the generation (or suppression) of hairpin vortices, (ii) to obtain information concerning the flow characteristics, in particular data that cannot be provided (at least easily) by experimental techniques.

NUMERICAL MODEL

Geometry and mesh

The computational domain is shown in Fig. 1. This domain models as closely as possible the experimental setup of Malkiel *et al.* (1999). A Couette flow is simulated between two concentric circular cylinders of radius 5 and 5.9 cm. The inner and outer cylinders rotate with an angular velocity of Ω_i and Ω_o (in the same direction), respectively, to produce a shear flow of a given strength. The symmetry of the problem is used to reduce the domain of calculation. The boundary opposite of the symmetry plane is placed at a distance of 2.5 cm. The upstream and downstream boundaries are placed at an angular position of 5° and 15° from the suction holes, respectively. Numerical experiments revealed that boundaries placed farther away (8° and 25°, respectively) did not affect the solution significantly in the region of interest. The flow disturbance is created by two square or circular suction holes (one on each side of the symmetry plane) with an area identical to that used in the experimental setup (3.5mm^2 total area). The center of each hole is placed at a distance of 3.5mm away from the symmetry plane.

A typical mesh consisted of 33×49×25 points in the radial, circumferential and axial directions, respectively. The mesh on the inner wall and on the symmetry plane is shown in Fig. 2. In several cases, unstructured meshes were employed (with approximately the same number of nodes). Mesh points were clustered in the hairpin vortex growth region.

Mathematical and discrete model

The incompressible time dependent Navier Stokes equations were solved by a commercial software package (Fluent, Fluent Inc.). The equations were solved in a rotating frame of reference rotating with a speed of the inner cylinder. On the upstream boundary as well as on the boundary opposite of the symmetry plane, the Couette velocity profile was specified. The inner and outer walls were rotating with the corresponding angular velocity.

The strength of the disturbance was controlled by the incoming Couette velocity profile (the rotational speeds Ω_i and Ω_o of the inner and outer cylinders and their radii, respectively) and the total volume flow rate through both suction holes that varied between $\dot{q} = 1$ to 6 cm^3/sec.

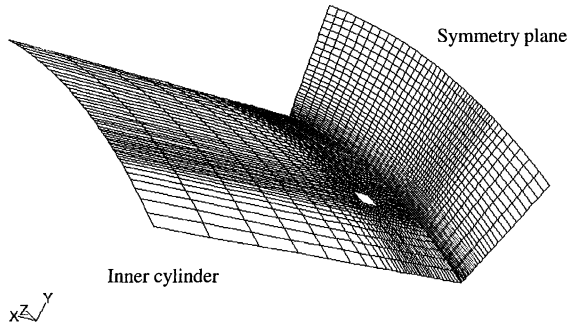

Figure 2: A sample mesh on the inner cylinder and on the symmetry plane.

A second-order upwind spatial discretization and an implicit first order temporal scheme were used. The SIMPLE approach was employed to decouple the continuity equation from the momentum equations. The discrete equations were solved by an algebraic multigrid method. A single time step required about 1min of Pentium II 300Mhz CPU time on an NT PC with 256 Mbyte memory for a mesh of approximately 40,000 nodes.

Validation

The solution was validated by performing mesh and time-step refinement tests that are summarized in Figs. 3-5. The tests were performed for the case of $\dot{q} = 1.5$ cm^2/sec and Ω_i =0, Ω_o =60rpm

The time step refinement test employed a mesh of approximately 40,000 nodes; the time step was varied between $\Delta t = 0.02$ and 0.000625 by halving it in each subsequent case. In Fig. 3 the evolution of the vorticity at a point on the symmetry plane is shown for all these cases. The peak corresponds to the instant when the hairpin center passes the point. Obviously, a time-step of $\Delta t = 0.0025$ is required to obtain a temporally converged solution. However, a large time step of $\Delta t = 0.005$ still results in an accurate solution.

Mesh independence was partially tested by refining the mesh in the region of the hairpin vortex evolution. In this region, the mesh size was decreased by half in each direction and the time step was fixed at $\Delta t = 0.0025$. The evolution of the vorticity at the same point is shown in Fig. 4 for the original mesh (Mesh 1, 40,000 nodes) and for a finer mesh (Mesh 2, 120,000 nodes). The finer mesh was generated by halving the mesh size in each direction in the region of the hairpin vortex growth. Noticeable differences can be observed only when the hairpin passes the test point.

To gain a better view on the significance of these differences, Fig. 5 gives the iso-vorticity surface for the two cases near the time of maximal difference in the vorticity (marked by square and circular symbols in Fig. 4). It should be noticed that in the presentation of these results, the solution is mirrored across the symmetry plane to show the two legs of the hairpin vortex. The shaded wall region below the hairpin marks the inner cylinder. The legs of the hairpin originate from the suction holes.

The form of the hairpin vortex is similar in both cases; however, the finer mesh results in a smoother surface and a more sharply defined vortex. Additional comparisons revealed that although local details may vary between the two meshes by as much as 20%, the global features, as well as all the physical processes, such as the evolution of the hairpin and its shedding are essentially mesh independent. Therefore in most of the simulations, the coarser mesh was employed.

RESULTS

The evolution of the hairpin from inception to its shedding is described in Fig. 6 for the case of $\dot{q} = 1.5$ cm^2/sec, Ω_i =0, Ω_o =60 rpm. The hairpin is visualized by plotting an iso-vorticity surface ($\omega = 130$ 1/sec) for several instants during one shedding cycle.

The hairpin starts as a disturbance concentrated near the inner cylinder spanning the two suction holes (the center of each suction hole is in the middle between the base of the hairpin leg and the small vorticity surface that extends in the direction opposite to the symmetry wall). The disturbance grows in size by penetrating into the outer flow, away from the inner cylinder. The head of the disturbance encounters a larger velocity of the shear flow. This difference in the velocity transforms the arc-like disturbance into a hairpin vortex by stretching the legs. The lift up induced by the legs of the vortex raises the hairpin head even more into the faster outer stream, until it is eventually pinched-off and is shed while the next hairpin is being built near the inner cylinder. Prior to the shedding, the lower part of the hairpin legs are stretched almost parallel to the wall (i.e. it is at a small angle with it), while the upper part of the legs has an inclination angle of 39° with the radial direction. This agrees very well with the theory (41°) and a with the experimental results (36°). A very similar sequence of the generation, growth and shedding of the hairpin was observed in the experiments as well.

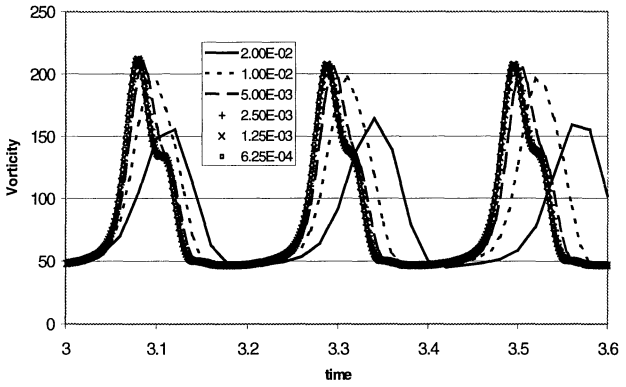

Figure 3: Time-step independence test of the vorticity

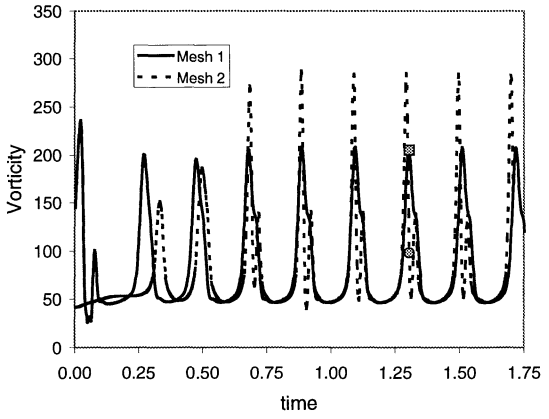

Figure 4: Mesh-independence test of the vorticity

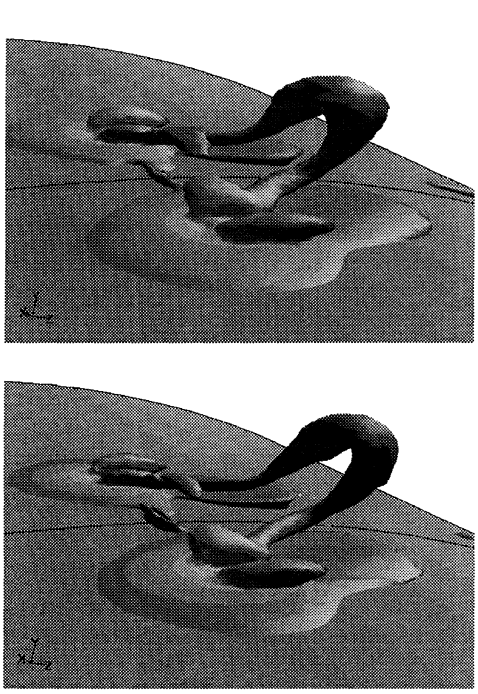

Figure 5: The hairpin at time=1.5 for the (a) coarse and (b) fine meshes

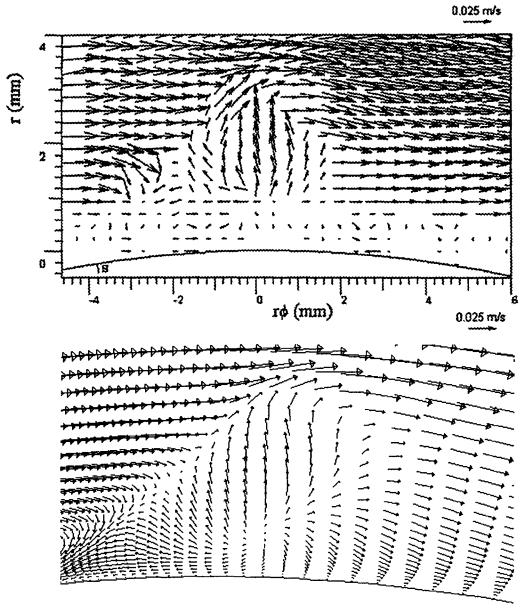

Figure 7: Comparison of the experimental and calculated velocity vector for the case of Ω_i =0, Ω_o =23 rpm and $\dot{q}$ = 1.5 cm^3/s

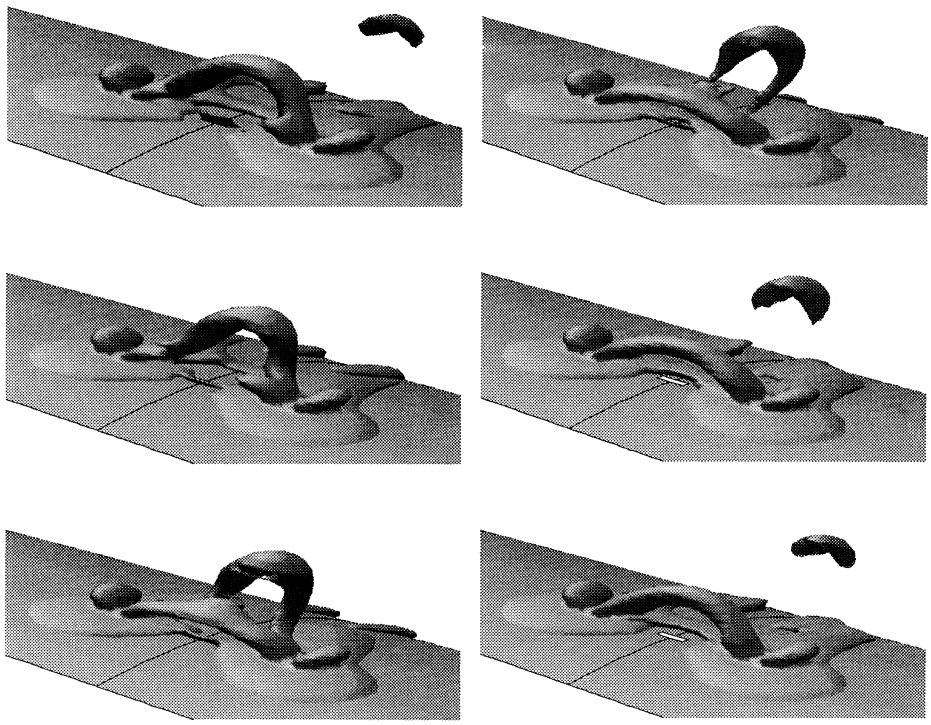

Figure 6: The evolution of a hairpin for the case of $\dot{q}$ = 1.5 cm^2/sec, Ω_i =0, Ω_o =60 rpm. The time difference between the plots is 0.06 sec. The shedding frequency is 3.3 Hz

The suction holes were introduced to generate the initial disturbance. Once a large enough disturbance is created, the above mentioned flow processes take care of transforming it into a hairpin vortex, provided the right conditions prevail (e.g., the flow is unstable, see the next section). Other generation methods of the initial finite-amplitude disturbance are possible, such as injection (Acarlar and Smith, 1987b) or finite-amplitude acoustic excitation leading to subcritical transition (Masahito and Nishioka, 1995) or roughness or hemisphere protuberance (Klebanoff *et al.* 1992, Acarlar and Smith, 1987a).

Comparison of the calculated velocity field on the symmetry plane with the experimental results is shown in Fig. 7 for the case of $\Omega_i = 0$ and $\Omega_o = 23$ rpm, $\dot{q} = 1.5$ cm^3/s. Good qualitative agreement is observed and the calculated flow field captured all the details observed in the PIV experimental data. It is worth noting that downstream of the suction holes (denoted by 's' in the upper plot), the fluid surrounding the hairpin is ejected outwards in the radial direction, away from the inner cylinder. This ejection, which resembles the bursting phenomenon observed in turbulent boundary layers, is in fact a superposition of the unperturbed flow and the flow induced by the hairpin.

The instability domain

In the experiments of Malkiel *et al.* (1999) an instability domain was found in the Ω_i/Ω_o and $\dot{q}$ domain for a given Ω_o and inner and outer radii. The term stability here means that the fluid impulse of a closed vortical disturbance (localized in all three directions) will not grow in time (see discussion in Malkiel *et al.*, 1999). In these experiments, hairpin vortices, similar to the ones reported for the case of a laminar boundary layer over a flat plate were found to develop in the instability region only. It should be recalled that in this instability region (in the Levinski and Cohen, 1995 sense) the flow is known to be linearly stable.

Figure 8 compares the instability region obtained experimentally (hollow symbols) with the calculated results (solid symbols). The instability region has a triangular shape in the Ω_i/Ω_o and $\dot{q}$ = plane. The lower boundary of the calculated results agrees very well with the experimental results. This boundary can be also theoretically predicted, Malkiel *et al.* (1999). Less favorable agreement is obtained in the upper boundary as well as in the right-most corner. Yet, the triangular shape of the region, that was an important discovery of the experiments of Malkiel *et al.* (1999) is obtained in the numerical simulations as well.

Outside of this triangular instability region, no hairpin evolution or shedding could be found. Typical forms of the disturbance are shown in Fig. 9 for three representing cases outside of the hairpin vortex growth instability region. In the first case, Fig. 9a, a low suction level is applied (Ω_i/Ω_o =0,

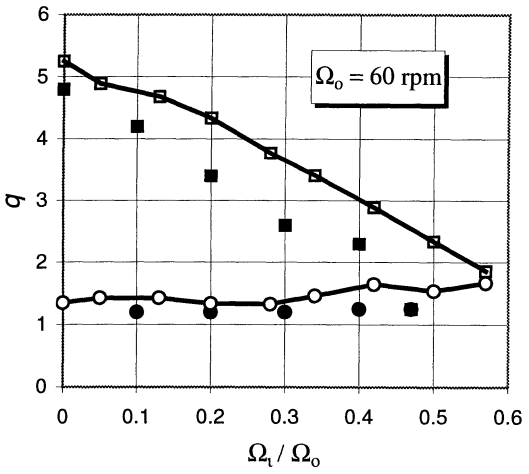

Figure 8: Comparison of the instability region (hairpin development region). Calculated results-solid symbols, experimental results- hollow symbols

$\dot{q} = 1$ cm^3/s). A disturbance is formed, yet it does not grow into a hairpin. Its central part, however, is shed, creating a slightly unsteady flow in this region.

Malkiel *et al.* (1999) estimated the perturbation size to grow as the square of ν (the kinematic viscosity). The lower stability bound (Fig. 8) should therefore depend on ν. In Fig. 10, the minimal suction rate (beyond which hairpin vortices grow) is plotted against a scaled kinematic viscosity (ν_{std} is the kinematic viscosity of water). Obviously, the minimal suction required for the growth of hairpin increases as the viscosity decreases (in the range of the calculations, the minimal suction is proportional to $1/\nu$). The dependence of the minimal suction rate on the viscosity found in the numerical simulations is in agreement with the theory.

CONCLUDING REMARKS

In the present study, numerical simulations of the inception, growth and shedding of hairpin vortices in rotating flows were compared with experimental results to validate the numerical model. An initial disturbance was created by suction. In the instability region (in the Ω_i/Ω_o and $\dot{q}$ = plane), the disturbance grows in size and it transforms into a hairpin vortex that is eventually shed, while another hairpin vortex is being formed. The numerical results are in good agreement with the experimental results. Thus, we developed and validated a numerical model for future study of the mechanisms involved in the hairpin evolution and shedding.

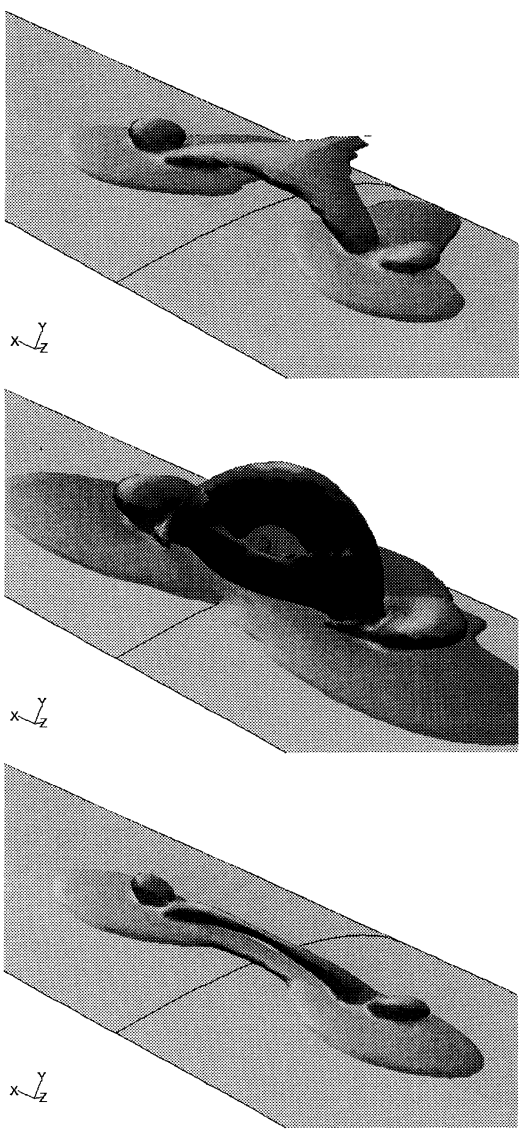

Figure 9: Iso-vorticity surfaces in the stable regions, (a) Ω_i / Ω_o =0, $\dot{q}$ = 1 cm^3/s, (b) Ω_i / Ω_o =0.3, $\dot{q}$ = 3 cm^3/s and (c) Ω_i / Ω_o =0.7, $\dot{q}$ = 1.5 cm^3/s

REFERENCES

Acarlar, M. S., and Smith, C. R., 1987a, "A study of hairpin vortices in laminar boundary layer. Part 1. Hairpin vortices generated by a hemispheric protuberance," *J. Fluid Mech,* Vol.. 175, 1.

Acarlar, M. S., and Smith, C. R., 1987b, "A study of hairpin vortices in laminar boundary layer. Part 2. Hairpin vortices generated by fluid injection," *J. Fluid Mech.* 175, 43.

Head, M. R., and Bandyopadhyay, P., 1981, "New aspect of turbulent boundary-layer structures," *J. Fluid Mech.*, 107, 297.

Kline, S.J., Reynolds, W.C., Schroub, F.A., and Runstadler, P.W., 1967, "The structure of turbulent boundary layers," *J. Fluid Mech.* 30, 741.

Levinski, V., and Cohen, J., 1995, "The evolution of a localized vortex disturbance in external shear flows. Part 1. Theoretical considerations and preliminary experimental results," *J. Fluid Mech.*, 289, 159.

Malkiel, E., Levinski, V., and Cohen, J., 1999, "The evolution of a localized vortex disturbance in external shear flows. Part 2. Comparison with experiments in rotating flows," *J. Fluid Mech.*, 379, 351.

Masahito, A. & Nishioka, M., 1995, Boundary-layer transition triggered by hairpin eddies at subcritical Reynolds numbers. *J. Fluid Mech.*, **297**, 101.

Moin, P. & Kim, J., 1985, The structure of the vorticity field in turbulent channel flow. Part 1: Analysis of the vorticity field and statistical correlations. *J. Fluid Mech.*, **155**, 441.

Zhou, J., Adrian, R. J. & Balachandar, S., 1996, Autogeneration of near-wall vortical structures in channel flow. *Phys. Fluids*, **8**, 288.